Growth Dynamics of Single-Wall Carbon Nanotubes Synthesized by CO_2 Laser Vaporization

F. Kokai,*,† K. Takahashi,† M. Yudasaka,§ R. Yamada,§ T. Ichihashi,‡ and S. Iijima§,‡

Institute of Research and Innovation, 1201 Takada, Kashiwa, Chiba 277-0861, Japan, Nanotubulite Project, JST-ICORP, c/o NEC Corporation, 34 Miyukigaoka, Tsukuba, Ibaraki 305-8501, Japan, and NEC Corporation, 34 Miyukigaoka, Tsukuba, Ibaraki 305-8501, Japan

Received: January 5, 1999; In Final Form: March 16, 1999

Single-wall carbon nanotubes (SWNTs) were synthesized by the irradiation of a 20-ms CO_2 laser pulse (1-kW peak power) onto a graphite−Co/Ni composite target at 25−1200 °C. Characterization of carbonaceous deposits using Raman scattering, scanning electron microscopy, and transmission electron microscopy showed that SWNTs were formed by laser irradiation even at room temperature. At 1100−1200 °C, the SWNT yield significantly increased (> 60%). A high-speed video imaging technique was used to observe the expanding vaporization plume and the emerging carbonaceous materials in an Ar atmosphere. Carbonaceous materials containing SWNTs became visible after ∼3 ms from the initiation of laser irradiation of the target. At 1000−1200 °C, blackbody emission from large carbon clusters and/or particles was observed for more than 1 s after the end of the laser pulse. We suggest that the growth of the SWNTs occurs from a liquidlike carbon−metal particle via supersaturation and segregation. A continuous supply of hot carbon clusters to the particles due to the 20-ms laser pulse and the maintenance of the hot growth zone for SWNTs, performed with the help of a furnace, are thought to play a crucial role in the SWNT formation.

Introduction

Since the discovery of single-wall carbon nanotube (SWNT),[1,2] various methods, including arc discharge,[3,4] laser ablation,[5−10] chemical vapor deposition,[11−13] and pyrolysis,[14,15] have been extensively applied to the synthesis of the SWNT. In these methods, graphite−metal composite, carbon monoxide and molybdenum, benzene and ferrocene, etc., are used as source materials. Because the coexistence of carbon and a small percentage of transition metal is required in the SWNT growth zone, catalytic growth is believed to be the mechanism of the SWNT formation.

In the studies using the laser ablation method, a single[5,7−9] or two successive[6,10] laser pulses with ns duration from Nd:YAG lasers were employed to ablate a graphite-metal composite target in a quartz cell installed in an electric furnace (1200 °C). More recently, Maser et al.[16] used a CO_2 laser operated in a continuous wave (CW) mode to form SWNTs. They found that SWNTs were produced even at room temperature. However, the role of reaction parameters, such as laser intensity and pulse duration, types and quantities of catalyst metals, and furnace temperature, is not fully understood. To control and improve the production process leading to high quality SWNTs on a large scale, it is essential to get a detailed understanding of the growth mechanism of the SWNTs. Furthermore, the temporal behavior of carbon and metal species ejected from a graphite−metal composite target is not well understood. It is necessary to investigate when and where SWNTs are formed during and/or after laser irradiation of the target.

In the present study, CO_2 laser pulses with a 20-ms duration and 1-kW peak power were used for laser vaporization of graphite−Co/Ni composite at 25−1200 °C. Similar to the result obtained by Maser et al.[16] using a CW CO_2 laser, characterization of carbonaceous deposits using Raman scattering, scanning electron microscopy (SEM), and transmission electron microscopy (TEM) show that the deposit contains SWNTs even at room temperature. We also found the yield of SWNTs in weblike deposits significantly increase when laser vaporization is done at 1100−1200 °C. In addition to characterization of the deposits, we performed diagnostics on the vaporization plume and carbonaceous materials in an Ar atmosphere using a high-speed video imaging technique and emission spectroscopy. These diagnostic techniques make it possible to trace the dynamic process of the SWNT growth. The growth mechanism of the SWNT is discussed in terms of the supply of hot carbon species and the temperature of the growth zone.

Experimental Section

The experimental apparatus for SWNT production used in this study was nearly identical to that used in our previous studies.[7,8] Briefly, our chamber for laser vaporization consists of double-layered quartz glass tubes. One tube has an inner diameter of 36 mm and a length of 600 mm, and the other tube has an inner diameter of 27 mm and a length of 500 mm. A Co/Ni−graphite composite pellet-like target (10 mm in diameter and 3−5 mm in thickness) was placed at the center of 27-mm tube by supporting it with a third quartz glass tube (10 mm in diameter and 300 mm in length). The concentrations of both Co and Ni were 0.6 atomic %. The target was kept at between 25 °C (room temperature) and 1200 °C using an electrical furnace.

A CO_2 laser beam (1-kW peak power and 20-ms rectangular pulse) was focused onto the target through a 510-mm focal

* Corresponding author. Telephone: (81) 471-44-8811. Fax: (81) 471-44-8939. E-mail: fkokai@iri.or.jp.
† Institute of Research and Innovation.
§ Nanotubulite Project, JST-ICORP.
‡ NEC Corporation.

10.1021/jp990065s CCC: $18.00
Published on Web 05/08/1999

length lens and a ZnSe window down to a 1-mm spot diameter. The laser power density on the target surface was estimated to be 1.3×10^5 W/cm^2. The SWNT synthesis was performed by single laser pulse irradiation. The Raman spectra of the carbonaceous deposits were measured using an Ar^+ ion laser with the wavelength of 488 nm. The spectral resolution was $\sim$5 cm^{-1}. Characterization by SEM and TEM of the carbonaceous deposit was performed as described in the previous papers.[7,8] The vaporization quantity of the target was estimated to be $\sim$0.1 mg from the weight loss of the target after an irradiation of 10 laser shots.

A high-speed video camera (Photoron FASTCAM-Rabbit) recorded the expanding vaporization plume and carbonaceous materials in an Ar atmosphere. The frame rate and shutter speed of the video camera were 600 s^{-1} and 10^{-4} s, respectively. For the high-temperature measurements, the cover of the furnace was slightly opened for 2−3 s. The decrease in temperature, monitored in the middle of the furnace, was about 50 °C for a setting temperature of 1200 °C.

The emission spectrum during the irradiation of the CO_2 laser was measured at right angles to the plume expansion with a 300-mm focal length lens that was able to be located at various points along the plume. The emission was imaged onto the entrance of the optical fiber of a photonic multichannel analyzer (Hamamatsu PMA-11). The spectrum was measured with an exposure time of 2 s and transferred to a personal computer with a correction for the detector's spectral response. The decay signal of the emission of carbon species in an Ar gas atmosphere was detected by a PIN silicon photodiode (Hamamatsu S1722−02) and stored on a digitizing oscilloscope (Hewlett-Packard 54111D). The image of the emission was focused on the detection surface of the photodiode by using a lens through the ZnSe window located at rear side of the target.

Results

A part of carbonaceous material formed by laser vaporization was deposited on the quartz tube wall in front of a graphite−Co/Ni target, and the remaining products flowed down to rear of the target. Between 1100 and 1200 °C, the amount of a sootlike deposit on the quartz tube wall in front of the target dramatically decreased, and a large amount of weblike material flowed down to the rear of the target and became attached to the inside the quartz tube near the exit of the furnace.

The Raman spectra of carbonaceous deposits obtained at four different temperatures are shown in Figure 1. The Raman spectra for the deposits at 25, 400, and 800 °C, obtained on quartz plates placed in front of the target, are similar. In the high-frequency region, a strong peak and a weak shoulder peak appear at 1591 and 1569 cm^{-1}, respectively. These two peaks are associated with the tangential C−C stretching modes of the SWNTs.[17] In the low-frequency region, there is a broad peak at around 180 cm^{-1} assigned to the band of the radial breathing mode.[17] These three peaks clearly indicate the presence of SWNTs in the deposits. The peak near 180 cm^{-1} is close to the 183 cm^{-1} peak of the armchair (9, 9) nanotube;[17] however, the broadness of the peak indicates that the SWNTs formed at 25, 400, and 800 °C are a mixture of SWNTs with different diameters. In addition to the three peaks, there is a broad peak due to non-SWNT carbon materials at 1350 cm^{-1}. Thus, the carbonaceous materials deposited at 25, 400, and 800 °C are composed of SWNTs and other carbon materials. Unlike the SWNT formation using Nd:YAG laser pulses, our results indicate that SWNT formation readily occurs by CO_2 laser vaporization at lower temperatures.

Like the Raman spectra for the deposits at 25, 400, and 800 °C, the Raman spectrum for a weblike deposit at 1200 °C has

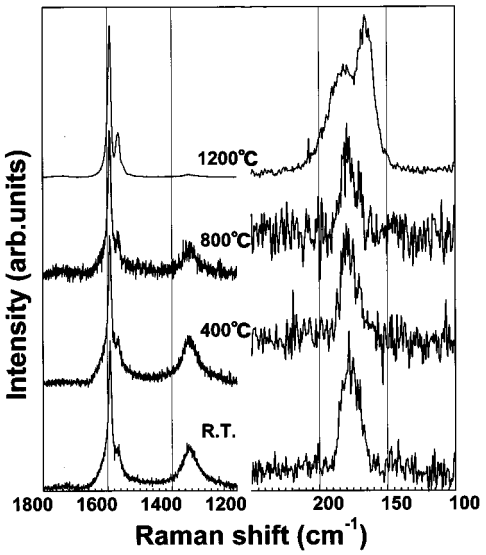

Figure 1. Raman spectra of carbonaceous deposits obtained by CO_2 laser vaporization of a graphite−Co/Ni composite target at temperatures of 25, 400, 800, and 1200 °C.

peaks at 1591 and 1569 cm^{-1} in the high-frequency part. However, the lower frequency part has a peak at about 165 cm^{-1} in addition to the peak at about 180 cm^{-1}. The peak at about 165 cm^{-1} is indicative of the formation of (10, 10) armchair-type SWNTs[17] with larger diameters. Bandow et al.[10] reported that the mean tube diameter increases with the increasing temperature in the growth zone. Our results for the deposits at 25−1200 °C are consistent with their results. Furthermore, the decrease in the relative intensity of the broad peak at about 1350 cm^{-1} for the deposit at 1200 °C indicates that the amount of SWNTs in our weblike deposit was quite high. These Raman scattering results are consistent with SEM and TEM examination of the deposits as follows.

Figure 2 shows typical SEM and TEM images of carbonaceous deposits obtained on quartz plates placed in front of the target at 25 °C. The SEM image shows the presence of SWNTs, together with a large amount of non-SWNT material. The TEM image also shows the presence of SWNTs, large carbon particles containing small Co/Ni particles (darkened regions), and other materials. Similar to previous observations,[7,8] a high-magnification TEM image showed that the SWNTs were in ropelike bundles. In Figure 2, in some of the SWNT bundles, we can observe one end of the bundle, which appears particle free. The other end is always found buried in the carbon−metal particle.

Figure 3 shows typical SEM and TEM images of the weblike deposit at 1200 °C. The SEM image shows that the amount of SWNTs significantly increases and that thicker bundles are produced at 1200 °C. In the TEM image, SWNT bundles with a multilane highway structure are observed. As seen in Figures 2 and 3, the yield of SWNTs was found to be very sensitive to the furnace temperature. Although SEM and TEM showed that the ratio of SWNTs to non-SWNT materials differs depending on the observation point in the weblike deposit, the yield of SWNTs were estimated to be more than 60% of the deposit in several SEM and TEM images.

A series of video images taken for the irradiation of a single 20-ms CO_2 laser pulse onto a graphite−Co/Ni composite target at 25 °C is shown in Figure 4. The distance from the target surface shown at the top of the figure. The generation of a long vaporization plume up to about 3 cm from the target surface can be seen in the images of 1.7−20.0 ms, which indicates that the ejection of carbon and metal species from the target

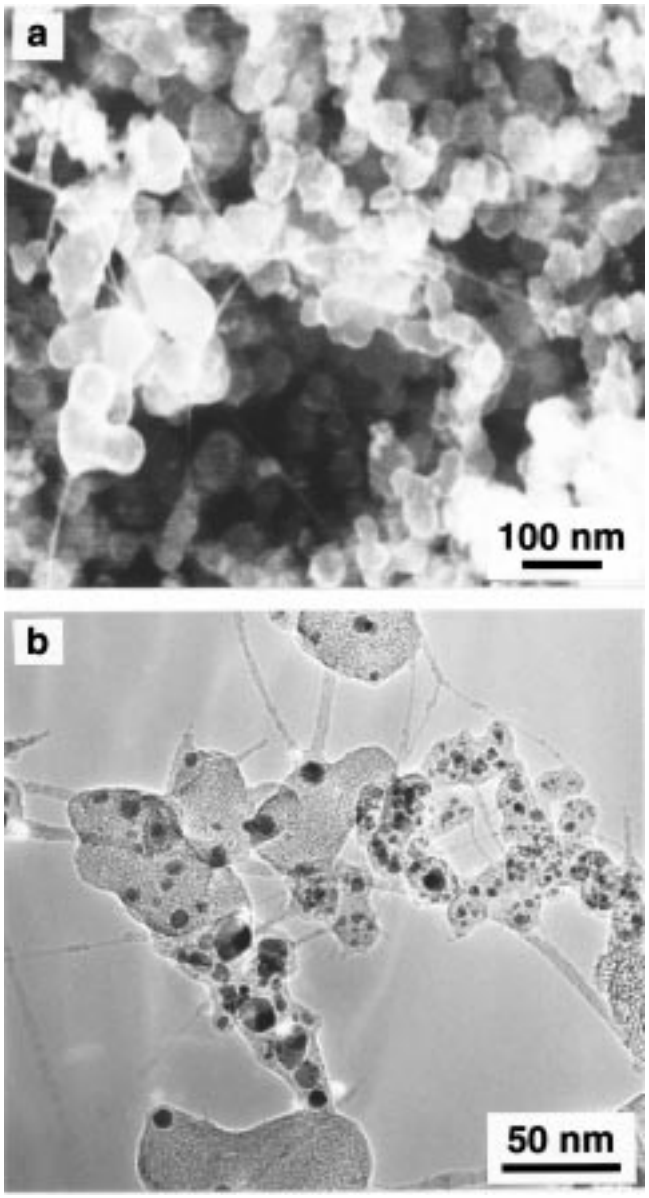

Figure 2. SEM and TEM images of a sootlike deposit produced by CO_2 laser vaporization at 25 °C.

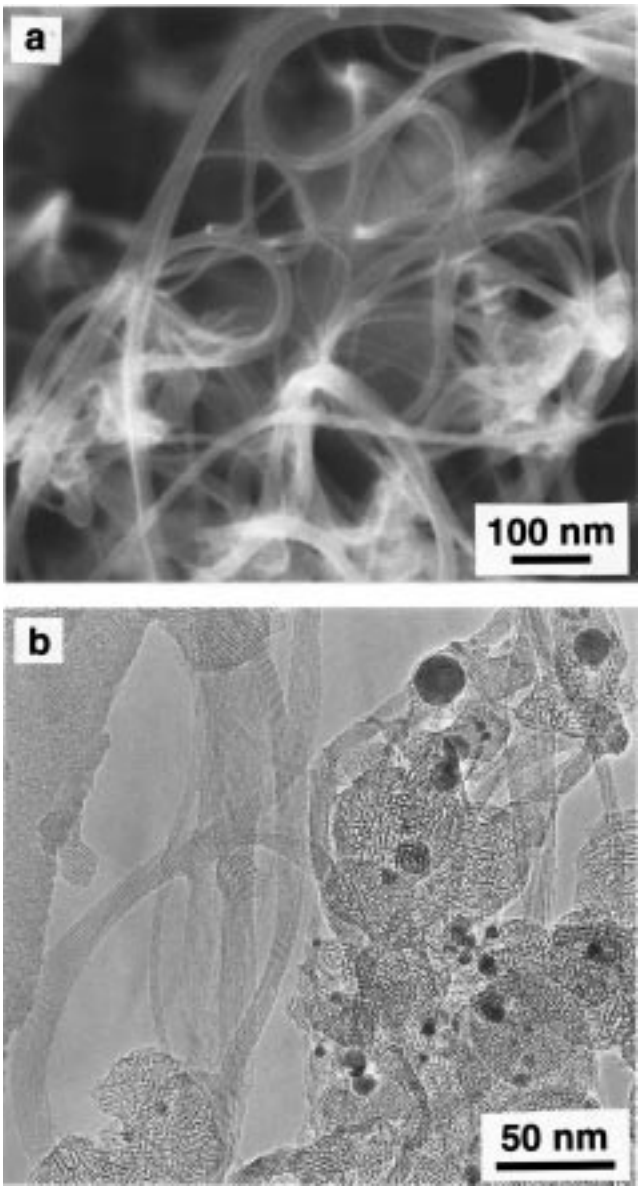

Figure 3. SEM and TEM images of a weblike deposit produced by CO_2 laser vaporization at 1200 °C.

continued for nearly 20 ms. The white part in the top of each image is due to the reflection of the plume on the quartz tube. The expansion velocity of the plume is estimated to be $\sim 1 \times 10^3$ cm/s from the 1.7- and 3.3-ms images. Compared to the expansion velocities of carbon species measured in Nd:YAG laser ablation,[18] $\sim 3.4 \times 10^5$ and $\sim 2.0 \times 10^5$ cm/s for C_2 and carbon particles, respectively, much slower expansion of carbon species occurs for the CO_2 laser irradiation probably due to a lower laser power density at the target surface. After 5 ms from the initiation of laser irradiation, turbulent plumes are found at a region of 2−4 cm from the target. In addition to the plume turbulence, emission along the incident CO_2 laser beam, which exists in a slightly narrower region than that of the vaporization plume, was observed at a region of 3−6 cm from the target. The plume turbulence and the emission seem to be due to the presence of soot-like materials formed in the flowing Ar gas. Indeed, the black materials are visible in the images taken at 3.00−20.0 ms (black materials can be seen more clearly at 1200 °C). The emission in front of the plume is due to blackbody emission from large carbon clusters and/or particles (containing metal particles) induced by CO_2 laser heating as mentioned below. After the end of laser irradiation, the irradiated spot region on the target is still hot and appears in the images at 21.7 and 23.3 ms.

To characterize the carbon species in the expanding plume seen in the video images, emission spectra were measured. Figure 5 shows the emission spectra of the plume measured at 15 and 25 mm from the target at 25 °C. The two spectra are dominated by continuum emission that peaks at 700−800 nm. Additionally, a weak C_2 Swan-band emission that peaks at 467, 516, and 560 nm, is present in the spectrum taken at 15 mm. The two origins of the formation of electronically excited C_2 molecules are recombinative production from two carbon atoms and collisional dissociation of large clusters induced by low-energy electrons in the plume.[18,19] The continuum emission, which seems to extend well into the near-infrared beyond 800 nm, can be attributed to blackbody emission from large carbon clusters[20] and carbon particles[18] (containing Co/Ni particles). We estimated the temperature of the carbon clusters and particles by fitting the continuum emission to the Plank blackbody distribution function. The fitted curves in Figure 5a and b give temperatures of 3540 and 3410 K, respectively. In addition, the

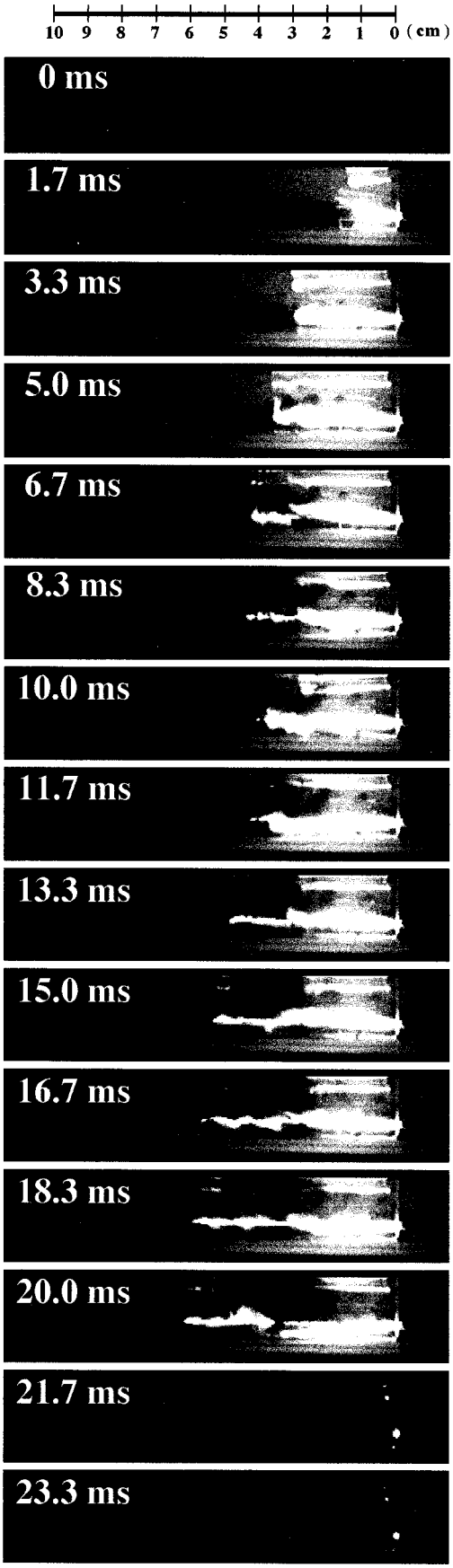

Figure 4. A series of video images of vaporization plume and carbonaceous material observed during and after CO_2 laser vaporization at 25 °C.

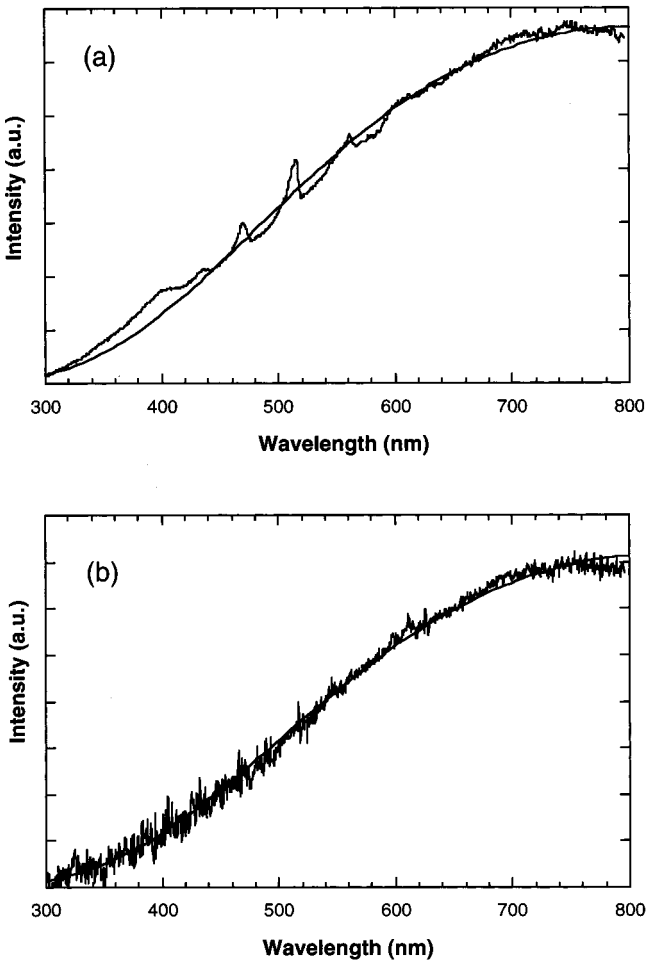

Figure 5. Emission spectra of vaporization plume observed at the positions of (a) 15 and (b) 25 mm from the target during CO_2 laser irradiation at 25 °C. The curves fitted with the Plank blackbody radiation function by assuming temperatures of (a) 3540 and (b) 3410 are also shown.

emission spectra taken at >25 mm from the target showed a continuum structure similar to that observed at 25 mm. Therefore, the emission along the incident laser beam in front of the vaporization plume results from blackbody emission induced by laser heating of cooled carbon clusters and particles. Laser-induced emission of carbon particles in a He gas atmosphere has been previously reported by Rohlfing.[18]

Figure 6 shows a series of video images recorded during CO_2 laser vaporization at 1200 °C. As in the case of the video images recorded at 25 °C, the ejection of carbon and metal species that accompanied the expanding plume occurs for nearly 20 ms. Plume turbulence and blackbody emission are also observed, and the area of the emission, particularly at 3−7 cm from the target, significantly increases, probably as a result of the increase in the number of carbon clusters and particles. Black carbonaceous materials probably containing SWNTs can clearly be seen near the emission area during the laser irradiation. After the laser irradiation, as can be seen in 21.7- and 23.3-ms images, high-density carbonaceous materials are present in the zone located at 3−8 cm from the target. As the Ar gas flew, the flowing nature of the carbonaceous materials (∼2 cm/s) was also observed in the quartz tube.

Like the emission spectra at 25 °C, blackbody radiation dominated the emission spectra at higher temperatures. However, the nature of the decay of the emission intensity was different. Figure 7 shows the time dependence of the emission intensity

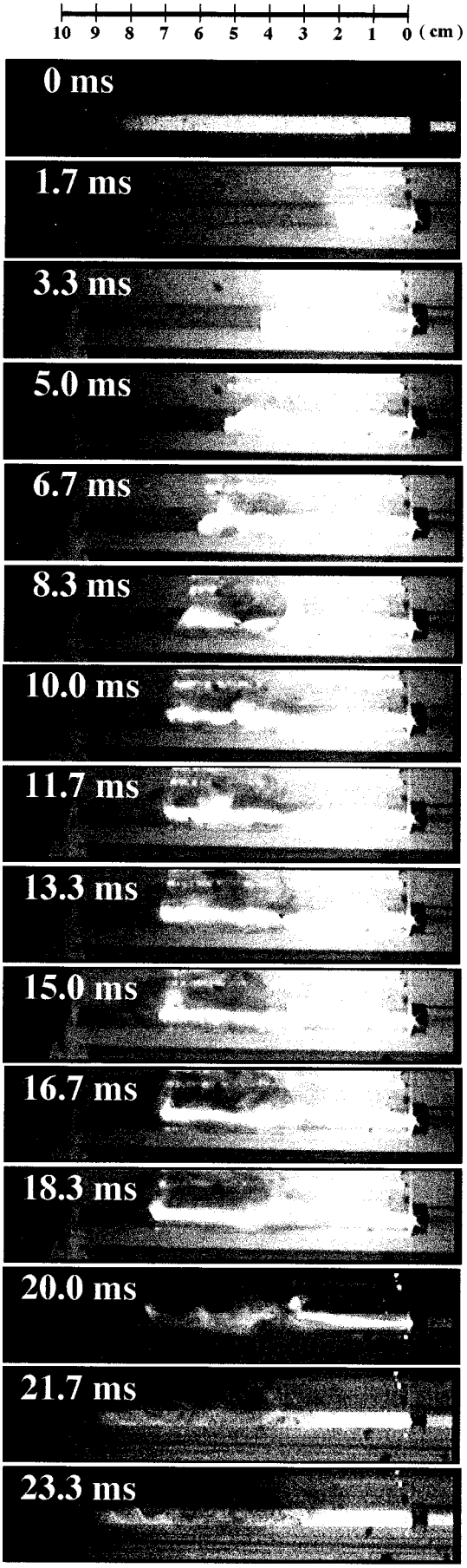

Figure 6. A series of video images of the vaporization plume and carbonaceous material observed during and after CO_2 laser vaporization at 1200 °C.

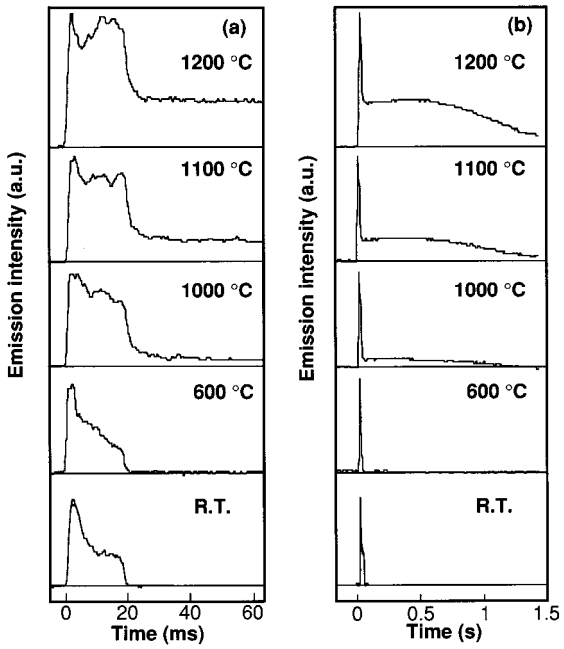

Figure 7. Time dependence of emission intensity during and after the irradiation of a 20-ms CO_2 laser pulse at 25, 600, 1000, 1100, and 1200 °C for (a) 0−60 ms and (b) 0−1.5 s.

measured by a photodiode during and after the irradiation of a 20-ms laser pulse at 25, 600, 1000, 1100, and 1200 °C. At all temperatures, there was a rapid increase followed by a rapid decrease in emission intensities after 20 ms that reflected the rectangular shape of the CO_2 laser pulse and decay of the plume emission. The emissions at 1000, 1100, and 1200 °C are stronger than those at 25 and 600 °C. More interestingly, after laser irradiation, extremely long-lived emission signals continuing more than 1 s are observed at 1000, 1100, and 1200 °C. This indicates that in an Ar gas atmosphere hot carbon clusters and/or particles exist near the target for a quite long time.

Discussion

The feature of ends of SWNT bundles and the presence of small Co/Ni particles embedded in large carbon particles in the TEM images (Figure 2) seems to indicates that a catalytic growth process, where a gas-phase molten particle composed of carbon and Co/Ni acts as a base and the growth of SWNTs occurs via supersaturation in carbon followed by its segregation, governs the growth mechanism of the SWNTs. An important role of molten carbon-metal particles is suggested for the SWNT formation using arc discharge[3] and laser ablation.[8]

Let us discuss how the molten particle forms and how supersaturation and segregation are brought about by CO_2 laser irradiation of a graphite−Co/Ni target. The majority of the carbon species ejected during CO_2 laser irradiation are thought to be C, C_2, C_3, or other small carbon clusters. Background Ar gas is thought to be key to the production of SWNTs after the ejection of the carbon species. First, the Ar gas atmosphere confines the vaporized carbon and metal species at early stages of the expansion of the vaporization plume, which leads to an enhanced collision frequency and subsequent growth of carbon and metal clusters at high temperature (∼3500 K). Second, dissipation of directed kinetic energies and cooling of the carbon and metal species occur by collisions with Ar atoms, which results in the growth of larger clusters and condensation of the clusters followed by the formation of droplet-like carbon-metal particles.[8] A kinetic-energy-dependent formation of carbon

clusters was suggested in laser ablation of polymers at different ablation laser wavelengths.[21] A formation of the Si particles from liquid droplets, which condense from Si vapor, was demonstrated for an arc discharge evaporation process.[22] More recently, for the growth of Si nanoparticles by laser ablation, it was suggested that the directed kinetic energies of Si atoms impede the formation of nuclei in a background gas.[23] Low solid solubilities of carbon,[24] 4.2 and 2.7 atomic % in Co and Ni, respectively, and the atomic composition of the graphite−Co/Ni target may govern the formation of Co/Ni particles surrounded by carbon. Third, as the droplets cool by the flowing Ar gas, the droplets become supersaturated in carbon and SWNT growth begins through the segregation of carbon. We believe that the maintenance of the supersaturation and segregation is strongly related to the supply of hot carbon clusters to the droplet and the temperature of the growth zone controlled by the furnace temperature. The length and the diameter of SWNT bundles depend very sensitively on the duration of the supersaturation and segregation. In the SWNT growth mentioned here, carbon species take on vapor, liquid, and solid states. A vapor−liquid−solid model was proposed as an explanation of how the silicon and germanium nanowires were formed by laser ablation.[25]

Unlike the SWNT formation process using Nd:YAG laser pulses in an electrical furnace, the SWNT formation observed for CO_2 laser irradiation at room temperature indicates that a favorable reaction condition for the SWNT growth was achieved. We believe that a hot SWNT growth zone is created even without the help of the furnace, because of the presence of the blackbody radiation (Figure 5). The supply of hot carbon clusters continuing for 20 ms during CO_2 laser vaporization is thought to play an important role in maintaining the supersaturation and segregation. In laser ablation by a Nd:YAG laser with a ns pulse duration, the supply of carbon species seems to occur for a shorter time than that by CO_2 laser vaporization. For example, a time-of-flight mass spectrometric measurement made during Nd:YAG laser ablation of graphite showed that ejected carbon species (major species were C, C_2, C_3, and their positive ions) arrived at a detection point, 45 mm from the surface of graphite, for time periods of only 6−35 μs.[26]

It is also worth noting that quite a high yield of SWNTs were observed at 1100−1200 °C in our experiment. The presence of prolonged emission (> 1 s) of carbon clusters and/or particles observed at 1000−1200 °C strongly supports the idea that the SWNT growth occurs as a result of hot metal−carbon particles accompanied by the supply of carbon species. As indicated in SWNT formation by arc discharge method,[3] there may be a time delay between the formation of the metal−carbon compound particle and the SWNT growth by segregation. The maintenance of hot metal−carbon particle produced by CO_2 laser vaporization performed with the help of a furnace is thought to enhance the growth of the SWNT. A small amount of Co/Ni particles in carbon−Co/Ni compound particles promotes the growth of SWNTs. The segregation of solid Ni and Co occurs at 1326.5 and 1321 °C from C−Ni and C−Co eutectics, respectively.[24] The temperature of the growth zone of the SWNT may be higher than 1200 °C.

Conclusion

Carbonaceous deposits, synthesized by the irradiation of a 20-ms CO_2 laser pulse on a graphite−Co/Ni composite target at 25−1200 °C, have been characterized by using Raman scattering, SEM, and TEM. The deposits contain SWNTs even with the target at room temperature. The yield of SWNTs in a weblike deposit was highest at 1100−1200 °C from SEM and TEM images. A yield of greater than 60% was estimated for laser vaporization at 1200 °C. We also performed diagnostics of vaporization plume and carbonaceous materials using a high-speed video imaging technique and emission spectroscopy. The dynamics of the expansion of the vaporization plume and the growth of carbonaceous materials were studied in an Ar atmosphere. Carbonaceous materials containing SWNTs were visible ~3 ms after initiation of laser irradiation of the target. At 1000−1200 °C, blackbody emission from large carbon clusters and/or particles was observed for more than 1 s after the end of the laser pulse. We discussed the growth mechanism of the SWNTs from a molten carbon−metal particle via supersaturation and segregation. We suggested that a continuos supply of hot carbon clusters and the maintenance of a hot SWNT growth zone are important.

Although our results suggested that catalytic growth of SWNT from carbon−metal particles had occurred, more work is needed to clarify the formation process of the carbon-metal particles and their detailed role in the SWNT growth.

References and Notes

(1) Iijima, S.; Ichihashi, T. *Nature* **1993**, *363*, 603.

(2) Bethune, D. S.; Kiang, C. H.; deVries, M. S.; Gorman, G.; Savoy, R.; Vazquez, J.; Beyers, R. *Nature* **1993**, *363*, 605.

(3) Saito, Y.; Okuda, M.; Tomita, M.; Hayashi, T. *Chem. Phys. Lett.* **1995**, *236*, 419.

(4) Journet, C.; Maser, W. K.; Bernier, P.; Loiseau, A.; Lamy de la Chapelle, M.; Lefrant, S.; Deniard, P.; Lee, R.; Fischer, J. E. *Nature* **1997**, *388*, 756.

(5) Guo, T.; Nikolaev, P.; Thess, A.; Colbert, D. T.; Smalley, R. E. *Chem. Phys. Lett.* **1995**, *236*, 419.

(6) Thess, A.; Lee, R.; Nikolaev, P.; Dai, H.; Petit, P.; Robert, J.; Xu, C.; Lee, Y. H.; Kim, S. G.; Rinzler, A. G.; Colbert, D. T.; Scuseria, G. E.; Tomanek, D.; Fischer, J. E.; Colbert, D. T.; Smalley, R. E. *Science* **1996**, *273*, 483.

(7) Yudasaka, M.; Komatsu, T.; Ichihashi, I.; Iijima, S. *Chem. Phys. Lett.* **1998**, *278*, 102.

(8) Yudasaka, M.; Komatsu, T.; Ichihashi, T.; Achiba, Y.; Iijima, S. *J. Phys. Chem. B* **1998**, *102*, 4892.

(9) Kataura, H.; Kimura, A.; Ohtuka, Y.; Suzuki, S.; Maniwa, Y.; Hanyu, T.; Achiba, Y. *Jpn. J. Appl. Phys.* **1998**, *37*, L616.

(10) Bandow, S.; Asaka, S. Saito, Y.; Rao, A. M.; Grigorian, L.; Richter, E.; Eklund, P. C. *Phys. Rev. Lett.* **1998**, *80*, 3779.

(11) Dai, H.; Rinzler, A. G.; Nikolaev, P.; Thess, A.; Colbert, D. T.; Smalley, R. E. *Chem. Phys. Lett.* **1996**, *260*, 471.

(12) Kong, J.; Cassell, A. M.; Dai, H. *Chem. Phys. Lett.* **1998**, *292*, 567.

(13) Mao, J. M.; Sun, L. F.; Qian, L. X.; Pan, Z. W.; Chang, B. H.; Zhou, W. Y.; Wang, G.; Xie, S. S. *Appl. Phys. Lett.* **1998**, *72*, 3297.

(14) Cheng, H. M.; Li, F.; Su, G.; Pan, H. Y.; He, L. L.; Sun, X.; Dresselhaus, M. S. *Appl. Phys. Lett.* **1998**, *72*, 3282.

(15) Satiskumar, B. C.; Govindaraj, A.; Sen, R.; Rao, C. N. R. *Chem. Phys. Lett.* **1998**, *293*, 47.

(16) Maser, W. K.; Munoz, E.; Beito, A. M.; Martinez, M. T. de la Fuente, G. F.; Maniette, Y.; Anglaret, E.; Sauvajor, J.-L. *Chem. Phys. Lett.* **1998**, *292*, 587.

(17) Rao, A. M.; Richter, E.; Bandow, S.; Chase, B.; Eklund, P. C. Williams, K, A.; Fang, S.; Subbaswamy, K. R.; Menon, M.; Thess, A.; Smalley. R. E.; Dresselhaus, G.; Dresselhaus, M. S. *Science* **1997**, *275*, 187.

(18) Rohlfing, E. A. *J. Chem. Phys.* **1988**, *89*, 6103.

(19) Anselment, M.; Smith, R. S.; Daykin, E.; Dimaruo, L. F. *Chem. Phys. Lett.* **1987**, *134*, 444.

(20) Geohegan, D. B.; Puretzky, A. *Mater. Res. Symp. Proc.* **1996**, *397*, 55.

(21) Kokai, F.; Koga, Y.; Kakudate, Y.; Kawaguchi.; Fujiwara, S.; Kubota, M.; Fukuda, K. *Appl. Phys. A* **1994**, *59*, 299.

(22) Iijima, S. *Jp. J. Appl. Phys.* **1987**, *26*, 357.

(23) Wood, R. F.; Leboeuf, J. N.; Chem, K. R.; Geohegan, D. B.; Puretzkey, A. A. *Appl. Surf. Sci.* **1998**, *127*, 151.

(24) Massalski, T. B. *Binary Alloy Phase Diagrams*; American Society for Metals: Metal Park, 1986.

(25) Morales, A. M.; Lieber, C. M. *Science* **1998**, *279*, 208.

(26) Kokai, F.; Koga, Y. *Nucl. Instrum. Methods B* **1997**, *121*, 387.